J. Fluid Mech. (1976), *vol.* 73, *part* 3, *pp.* 497–520
Printed in Great Britain

A numerical study of the temporal eigenvalue spectrum of the Blasius boundary layer

By LESLIE M. MACK
Jet Propulsion Laboratory, California Institute of Technology, Pasadena

(Received 14 October 1974 and in revised form 15 September 1975)

A numerical study is made of the temporal eigenvalue spectrum of the Orr–Sommerfeld equation for the Blasius boundary layer. Unlike channel flows, there is no mathematical proof that this flow has an infinite spectrum of discrete eigenvalues. The Orr–Sommerfeld equation is integrated numerically, and the eigenvalues located by tracing out the contour lines in the complex wave velocity ($c = c_r + ic_i$) plane on which the real and imaginary parts of the secular determinant are zero. This method gives only a finite and small number of discrete eigenvalues for a wide range of Reynolds numbers and wavenumbers. The spectrum of plane Poiseuille flow is used as a guide to study the spectrum of an artificial two-wall flow which consists of two Blasius boundary layers. As the upper boundary of this flow moves to infinity, it is found that the portion of the spectrum with an infinite number of eigenvalues moves towards $c_r = 1$ and the spacing between eigenvalues goes to zero. It is concluded, on the basis of this result and the contour method, that the original few eigenvalues found are the only discrete eigenvalues that exist for Blasius flow over a wide portion of the c plane for $c_r < 1$ and $c_r > 1$. It is suggested that the discrete spectrum is supplemented by a continuous spectrum which lies along the $c_r = 1$ axis for $c_i < -\alpha/R$.

1. Introduction

Numerous investigations have been carried out on the temporal eigenvalue spectrum of the Orr–Sommerfeld equation for plane Couette flow (Gallagher & Mercer 1964), plane Poiseuille flow (Grosch & Salwen 1968; Orszag 1971) and axisymmetric Poiseuille flow (Davey & Drazin 1969; Salwen & Grosch 1972). In contrast, until the appearance of the note by Jordinson (1971), only the fundamental, or Tollmien–Schlichting mode, had been studied for boundary-layer flow. Perhaps one reason for this lack of attention is that the boundary layer does not offer as well posed a mathematical problem as does Couette or Poiseuille flow. Not only is the boundary layer not an exact solution of the Navier–Stokes equations, but a further approximation beyond linearization, that of locally parallel flow, is needed to arrive at the Orr–Sommerfeld equation. The additional complication of not having a finite interval has so far precluded any general mathematical analysis, such as has been carried out by Schensted (1960) and DiPrima & Habetler (1969) for finite-interval Orr–Sommerfeld problems. Nevertheless, the stability of boundary-layer flows has been studied for over 50 years on the

basis of the Orr–Sommerfeld equation, and the results obtained have much experimental support. It has always been assumed that an infinite sequence of discrete eigenvalues exists (see Betchov & Criminale 1967, p. 120), and that any arbitrary disturbance can be represented by an infinite series of the eigenmodes. However, no concrete evidence of an infinite eigenvalue spectrum has yet been brought forward.

It is the purpose of the present paper to examine the problem of the eigenvalue spectrum of the Blasius boundary layer by a numerical method different from that used by Jordinson (1971). This method is described in §2. The results presented in §3 show a discrete spectrum which differs from Jordinson's as to the number and location of the modes, but does agree to the extent that there are only a small number of them. Detailed results are given concerning the dependence of the location and number of the modes on the wavenumber α and Reynolds number R. Particular attention is paid to the limits $R \to 0$ and $R \to \infty$ with α constant, and $\alpha \to 0$ with R constant.

In an effort to understand why so few eigenvalues are obtained, some calculations for symmetrical channel flows are presented in §4. Schensted (1960) and DiPrima & Habetler (1969) proved that in a finite interval there is an infinite discrete spectrum for any velocity profile. The first few modes of the part of the spectrum of plane Poiseuille flow that contains an infinite number of eigenvalues (called the S family) are computed, and used as a guide in two artificial flow problems where the behaviour of these modes is studied as the upper wall moves to infinity and the height of the shear layer remains constant. The limiting behaviour is found to depend upon the velocity profile. With a parabolic profile the spectrum remains discrete and apparently infinite; for a Blasius profile the S family moves towards $c_r = 1$. (c_r is the phase velocity.) In §5 calculations are presented for two families of polynomial profiles in order to study the effect of discontinuities in the velocity derivatives at the outer edge of the boundary layer. These calculations suggest that when the velocity profile is sufficiently smooth at the outer edge, the discrete spectrum is finite. Finally, in §6 the possibility of a continuous spectrum for Blasius flow located along $c_r = 1$, $c_i < -\alpha/R$ is considered. It is suggested that such a spectrum does exist, provided that both viscous solutions are used and that the amplitudes of the two solutions in the free stream are not required to be equal.

2. Numerical methods

The basic numerical method is one that has been employed successfully in the study of the stability of the compressible boundary layer. An early account may be found in Mack (1965). For a two-dimensional sinusoidal disturbance in a two-dimensional mean flow, or more generally with an appropriate transformation, the linearized Navier–Stokes equations of the parallel-flow model reduce to the four first-order differential equations

$$f' = g, \tag{1}$$

$$g' = [iR(\alpha U - \omega) + \alpha^2]f + \alpha R U' \phi + i\alpha R \pi, \tag{2}$$

$$\phi' = -if, \tag{3}$$

$$\pi' = -i\frac{\alpha}{R}g - \alpha\left[i(\alpha U - \omega) + \frac{\alpha^2}{R}\right]\phi. \tag{4}$$

$f(y)$, $\alpha\phi(y)$ and $\pi(y)$ are the complex amplitude functions of $\hat{u}$, $\hat{v}$ and $\hat{p}$, the longitudinal velocity, normal velocity and pressure fluctuation, respectively. $U(y)$ is the mean velocity, α the wavenumber and ω the frequency. All quantities are made dimensionless with respect to the length scale L^* and velocity scale U_1^*. The Reynolds number R is $U_1^* L^*/\nu^*$. Asterisks refer to dimensional quantities, and the subscript 1 to free-stream quantities. The primes refer to d/dy, where y is the dimensionless independent variable y^*/L^*. For the Blasius boundary layer,

$$L^* = x^*/R_x^{\frac{1}{2}}, \quad \text{where} \quad R_x = U_1^* x^*/\nu^*,$$

and y becomes the Blasius variable $y^* R_x^{\frac{1}{2}}/x^*$ and R becomes $R_x^{\frac{1}{2}}$. For a parabolic velocity profile, the maximum velocity U_1^* is located at $y^* = L^*$, and for the problems treated in § 4, L^* is the channel half-width only for Poiseuille flow.

The first-order equations (1)–(4) are an alternative way of writing the fourth-order Orr–Sommerfeld equation. The present formulation was adopted because the incompressible case is an option in the author's large computer program VSTAB, which was set up originally for compressible flow, where it is not possible to write a single differential equation. The boundary conditions at the lower boundary are

$$f(0) = 0, \quad \phi(0) = 0. \tag{5}$$

With no second boundary, the upper boundary conditions are

$$f, \phi, \pi \quad \text{bounded as} \quad y \to \infty. \tag{6}$$

With a second boundary at $y = 2H$, the upper boundary conditions are replaced by conditions on the symmetry axis located at $y = H$. For an antisymmetric disturbance,

$$f(H) = 0, \quad \phi(H) = 1; \tag{7a}$$

and, for a symmetric disturbance,

$$f(H) = 1, \quad \phi(H) = 0. \tag{7b}$$

The symmetry referred to here is the symmetry of the physical disturbance, which is symmetric or antisymmetric in the same sense as the mean flow.

Instead of applying the boundary conditions (6) directly, the differential equations are solved analytically in the free stream where $U = 1$ and $U' = 0$, and the two solutions selected which satisfy the boundary conditions. These solutions provide the initial conditions for the numerical integration, which will proceed over the finite interval from some point y_1 to the wall. The four solutions are of the form $\exp(\lambda y)$, and the values of λ are

$$\lambda_{1,2} = \mp\alpha, \quad \lambda_{3,4} = \mp p, \tag{8}$$

where

$$p = [\alpha^2 + iR(\alpha - \omega)]^{\frac{1}{2}}, \quad \mathrm{Re}\,(p) \geqslant 0. \tag{9}$$

Solutions 1 and 2 are the inviscid solutions; 3 and 4 the viscous solutions. The corresponding amplitude functions are

$$f^{(1),(2)} = \mp i\alpha \exp(\mp \alpha y), \qquad f^{(3),(4)} = \mp ip \exp(\mp py), \tag{10}$$

$$g^{(1),(2)} = i\alpha^2 \exp(\mp \alpha y), \qquad g^{(3),(4)} = ip^2 \exp(\mp py), \tag{11}$$

$$\phi^{(1),(2)} = \exp(\mp \alpha y), \qquad \phi^{(3),(4)} = \exp(\mp py), \tag{12}$$

$$\pi^{(1),(2)} = \pm i(\alpha - \omega) \exp(\mp \alpha y), \quad \pi^{(3),(4)} = 0. \tag{13}$$

The appropriate solutions to use to satisfy the boundary conditions at $y \to \infty$ are 1 and 3, i.e. the upper signs of (10)–(13). The initial conditions of the numerical integration are given by (10)–(13) evaluated at $y = y_1$. The initial conditions could also be taken as (10)–(13) without the exponential factors, in which case the initial values would be independent of y_1. However, with (10)–(13) as written, the initial *solutions* are independent of y_1 and this feature turns out to be advantageous in the method to be explained below for finding the eigenvalues.

With a second boundary at $y = 2H$ all four solutions are needed. The appropriate form of solutions 2 and 4 for an antisymmetric disturbance are

$$f^{(2)} = i\alpha \exp[-\alpha(2H-y)], \qquad f^{(4)} = ip \exp[-p(2H-y)], \tag{14}$$

$$g^{(2)} = i\alpha^2 \exp[-\alpha(2H-y)], \qquad g^{(4)} = ip^2 \exp[-p(2H-y)], \tag{15}$$

$$\phi^{(2)} = \exp[-\alpha(2H-y)], \qquad \phi^{(4)} = \exp[-p(2H-y)], \tag{16}$$

$$\pi^{(2)} = i(\alpha-\omega) \exp[-\alpha(2H-y)], \quad \pi^{(4)} = 0, \tag{17}$$

and the signs are reversed for a symmetric disturbance. The initial conditions are the sums of solutions 1 and 2 and of 3 and 4 evaluated at $y = y_1$. Thus, even with two boundaries it is still necessary to integrate numerically only two solutions.

A forward integration method is used to integrate (1)–(4) from the starting point y_1 to the wall at $y = 0$ for given values of α, R and ω. Both solutions are integrated at the same time, which makes a total of 8 complex or 16 real equations. Three different double-precision integrators are available in VSTAB, and were used at various times in this investigation. They are: (i) a fourth-order fixed step-size Runge–Kutta integrator; (ii) a fixed step-size, fixed-order (1–8) Adams–Moulton integrator with a Runge–Kutta starter; and (iii) a variable step-size, variable-order self-starting Adams–Moulton integrator equipped with a variety of error tests. The majority of the calculations were done with the Runge–Kutta integrator because of its greater stability, but the additional integrators were useful in resolving questionable eigenvalues. The problem of spurious eigenvalues is a serious one in a numerical investigation of this type, and no eigenvalues were considered definitely established unless they could be produced by all three integrators.

The round-off error problem that arises when the growth of the λ_3 solution is so large as to destroy the linear independence of the two solutions is eliminated by use of the Gram–Schmidt orthonormalization procedure. If S is the four-component complex solution vector (f, g, ϕ, π) and the Euclidean norm $\{S^*S\}^{\frac{1}{2}}$ is

used (S^* refers to the complex conjugate vector), the original vectors $S^{(1)}$ and $S^{(3)}$ are replaced by

$$\bar{S}^{(3)} = S^{(3)}/\{S^{(3)*}S^{(3)}\}^{\frac{1}{2}}, \tag{18a}$$

$$\bar{S}^{(1)} = [S^{(1)} - \{\bar{S}^{(3)*}S^{(1)}\}\bar{S}^{(3)}]/\{\bar{S}^{(1)*}\bar{S}^{(1)}\}^{\frac{1}{2}}. \tag{18b}$$

$\bar{S}^{(1)}$ refers to the quantity in the preceding square brackets. This procedure allows eigenvalues to be computed for solution growths of over 10^{200} with a computer that carries 18 decimal digits. As the phase velocity $c_r = \omega_r/\alpha$ increases towards unity, a value of c_r is eventually reached where the growth of the λ_3 solution ceases to be a problem and orthonormalization is no longer needed. However, there can also be a c_r, particularly at large Reynolds numbers, where for sufficiently large negative c_i ($= \omega_i/\alpha$) it proves to be no longer possible to integrate the λ_3 solution with sufficient accuracy to determine eigenvalues. This loss of accuracy, which is unrelated to the step size, appears to come from a region where the λ_3 solution *decreases* several orders of magnitude at the same time as the λ_4 solution *increases* a like amount. Consequently, when the growth of the λ_4 solution relative to the λ_3 solution equals the number of significant digits in the computer word, all accuracy is lost in the λ_3 solution. It does no good to orthonormalize the λ_3 solution with respect to the λ_4 solution, although such a solution can be integrated accurately, because the orthonormalization is based on an arbitrarily selected norm of the vector space, and the orthonormalized vectors are not orthogonal in a true geometric sense. Thus, the orthonormalized solution which replaces the λ_3 solution is not free of any component of λ_4, as the geometric analogy would suggest, but is a linear combination of the λ_3 and λ_4 solutions. This cannot be used to satisfy the boundary conditions at $y = 0$, which require only the λ_1 and λ_3 solutions. The unfortunate result of this behaviour is that there is a region of the complex c ($= \omega/\alpha$) plane that is not accessible to the present numerical method.

At $y = 0$ a linear combination of the λ_1 and λ_3 solutions, or their orthonormalized counterparts, satisfies the boundary condition $f(0) = 0$ and the arbitrary amplitude condition $\pi(0) = (1, 0)$. Additional integrations are carried out within the framework of a Newton–Raphson search procedure until an ω (or c) is found for the specified α and R which satisfies the second boundary condition $\phi(0) = 0$. Even though the scalar products of the orthonormalization use the complex conjugate solution vectors, the function $\phi(0)$, or the secular determinant $D(0)$, is still either an analytic function of c or numerically indistinguishable from an analytic function. Thus the Cauchy–Riemann equations can be used, and only a single perturbation integration is required for each iteration.

The boundary-layer profiles were computed by a separate program, and stored as tables with a spacing of $\Delta y = 0{\cdot}1$. In this computation the outer boundary conditions were satisfied at $y = 15{\cdot}0$, and the per-step error limit of the variable step integrator was set at 10^{-15}. The resulting tables are smooth out to $y = 15{\cdot}0$, but U' has no more significant digits beyond $y = 13{\cdot}7$. In order to improve the profiles at large y and increase the allowable y range, the first term of the asymptotic expansion given by Blasius (1908),

$$U' = 1 - \gamma \exp[-\tfrac{1}{4}(y - \delta^*)^2], \tag{19}$$

was fitted to the calculated value of U' at $y = 11{\cdot}2$. With $\delta^* R_x^{\frac{1}{2}}/x = 1{\cdot}7207876$, the constant γ was found to be 0·23372766. The velocity U is easily calculable from the complementary error function.

An essential part of any numerical method is a systematic procedure for finding all of the eigenvalues in a given region of the complex c or ω planes. The automatic linear search procedure operates in a manner unpredictable with respect to its radius of convergence, and cannot be used for this purpose. An attempt was made to use the eigenvalue test quantity $\phi(0)$: first, by examining its magnitude as a function of c at a fixed α and R; and, second, by tracing out the contours of zero real and imaginary parts and looking for intersection points. The first method is unreliable, and the second has the disadvantage that the closed contours of small radius obtained in some regions require a great many calculation points to locate. Furthermore, only one-half of the intersection points are eigenvalues, with the remaining one-half being singularities of the function $\phi(0)$. Finally, the method used by Raetz (1966) and also by Kümmerer (1973) was adopted. In this method, the complex secular determinant

$$D(0) = \begin{vmatrix} f^{(1)}(0) & \phi^{(1)}(0) \\ f^{(3)}(0) & \phi^{(3)}(0) \end{vmatrix} \tag{20}$$

is computed at enough points in the c plane so that contours of $D_r = 0$ and $D_i = 0$ can be drawn. Intersection points of the real and imaginary contours locate possible eigenvalues which are then checked by the automatic search procedure. This method is tedious, and is sometimes impracticable because of the large number of contours; but it has the considerable advantage that no eigenvalues are known that are not intersection points, and no intersection points have yet been found that are not eigenvalues.

3. Eigenvalues of the Blasius boundary layer

3.1. *Eigenvalues at* $\alpha = 0{\cdot}179$, $R = 580$

The secular determinant was calculated at a large number of values of c at $\alpha = 0{\cdot}179$, $R = 580$† with a Univac 1108 computer (72 bit double-precision word) in order to establish the contours of $D_r = 0$ and $D_i = 0$. The contours obtained with initial conditions (10)–(13) are shown in figure 1 for $0 \leqslant c_r \leqslant 1$, $-0{\cdot}8 \leqslant c_i \leqslant 0{\cdot}1$. Along the solid lines $D_r = 0$, and along the broken lines $D_i = 0$. Except at the intersection points, the contours are located only approximately, since they were hand drawn from sometimes widely spaced grid points. However, enough grid points were used to establish the correct number of sign changes in D_r and D_i in all parts of the c plane.

The one intersection point for $c_i > 0$ is called mode 1 and is the unstable

† These values of α and R constitute (approximately) the temporal case considered by Jordinson (1971), where the α and R based on displacement thickness, α_{δ^*} and R_{δ^*}, were 0·308 and 998, respectively. In accordance with the definitions given in § 2, the α and R of this paper are to be multiplied by the dimensionless displacement thickness $\delta^* R_x^{\frac{1}{2}}/x^*$ to give α_{δ^*} and R_{δ^*}.

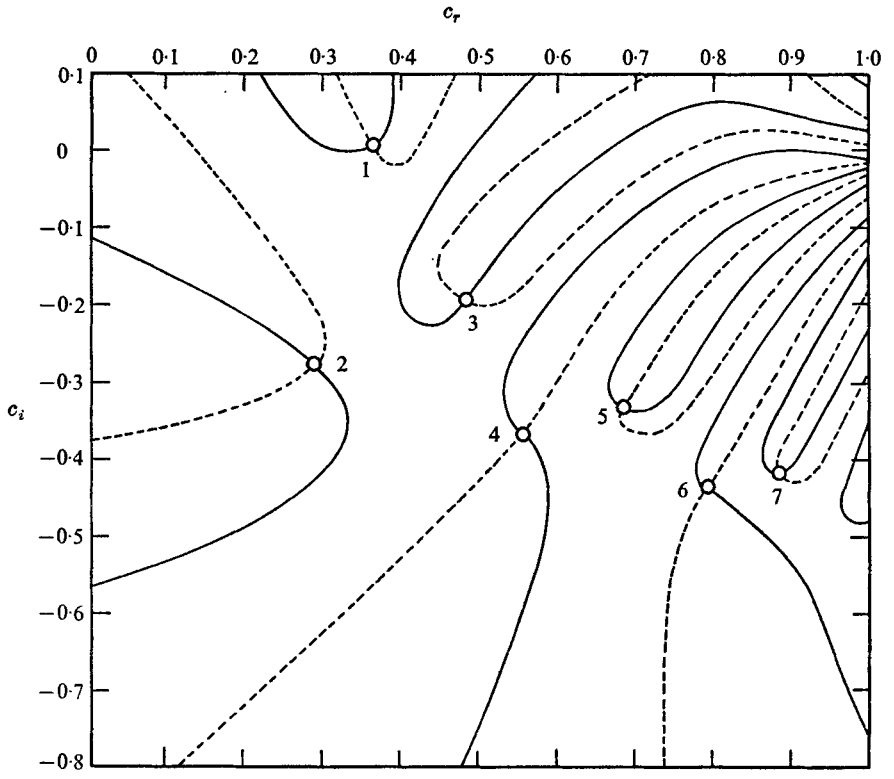

FIGURE 1. Zero contour lines of secular determinant for Blasius flow at $\alpha = 0{\cdot}179$, $R = 580$: ——, $D_r = 0$; – – –, $D_i = 0$.

Tollmien–Schlichting disturbance. For $c_i < 0$, there are a total of six intersection points. They are numbered in the order of increasing c_r because it is this order, rather than that with respect to c_i, which the numerical results to be presented later show is independent of α and R. The contours shown are the only ones that exist in the part of the c plane included in the figure. If the initial conditions are taken to be (10)–(13) without the exponential factors, the whole c plane is filled with contours whose spacing is inversely proportional to y_1. Only a few of these contours lead to intersections, since the intersection points must still be those shown in figure 1. The advantage of the present method of defining the initial values is that only a limited number of contours exist, and on each contour there is one and only one intersection point. However, some of the intersections may occur only for $c_r > 1$, as happens with the partial contour that appears near $c_r = 1$ in the lower right-hand part of figure 1. These intersections do not represent proper eigenvalues. As is evident from an inspection of (9), when $c_i < \alpha/R$ continuity of the viscous solution, and thus continuity of the contours, requires the use of the λ_4 viscous solution when $c_r > 1$ rather than the λ_3 solution. The λ_4 solution does not satisfy the boundary conditions (6) as $y \to \infty$. With the λ_3 viscous solution, the contours for $c_r > 1$ bear no relation to those for $c_r < 1$.

These contours are for the most part widely spaced, and since they diverge as c_r and $-c_i$ increase no intersections are likely anywhere for $c_r > 1$. For $c_r < 1$, the three contours which cross $c_i = -0{\cdot}8$ end up at either $c_r = 0$ (the two left-most contours) or at $c_r = 1$ (the $D_i = 0$ contour to the right). There are no other contours down to at least $c_i = -3{\cdot}0$, and at this c_i the secular determinant is almost constant for all c_r (except possibly near $c_r = 1$, where the integration breaks down).

The seven intersection points of figure 1, which were originally located only approximately by the contour method, were computed accurately by the automatic search procedure. The results are listed in table 1. Since the magnitude of $\phi(0)$ was reduced to at least 1×10^{-6} by the search procedure, the intersection points are confirmed to be eigenvalues. The interest in doing these calculations was more in finding the eigenvalues than in providing precise numerical values.† A step size s of 0·1 is sufficient for this purpose for all modes at $R = 580$. The step size listed in the table is roughly the largest that will produce four-place accuracy with the Runge–Kutta integrator. The value of y_1, the starting point of the numerical integration, is not critical except when c_r starts to approach unity. For $R = 580$, $y_1 = 8$ is adequate for modes 1–6, and $y_1 = 10$ for mode 7.

3.2. *Effect of Reynolds number and wavenumber on eigenvalues*

With the eigenvalues known at $\alpha = 0{\cdot}179$, $R = 580$, it was not difficult to extend the calculations by extrapolation to other Reynolds numbers with α remaining fixed. It was found that with increasing R each eigenvalue moves to a smaller c_r and $-c_i$. A search for additional eigenvalues at $R = 1000$ in the region between mode 7 and $c_r = 1$ yielded three more eigenvalues. The 10 eigenvalues are shown in figure 2 (*a*) and listed in table 1. They form the same kind of pattern as at $R = 580$. The odd-numbered modes lie along an 'upper line', and the even-numbered modes along a 'lower line'. These two lines are only slightly displaced from similar lines which could have been drawn in figure 1. Consequently, as the Reynolds number increases with α fixed, all eigenvalues move to the left essentially along the two lines, and new eigenvalues appear at the $c_r = 1$ boundary, first on one line, then on the other. These new eigenvalues are actually the 'eigenvalues' mentioned previously that can be calculated for $c_r > 1$ with the λ_4 solution. At $R = 1000$, $y_1 = 8$ is sufficient for all eigenvalues up to and including mode 8; $y_1 = 10$ is required for better than three-place accuracy in mode 9, but gives no convergence at all for mode 10. Convergence is obtained for mode 10 with $y_1 = 12$, but the eigenvalue does not become independent of y_1 until $y_1 = 14$.

A further increase of R to 2000 yielded the results shown in figure 2 (*b*) and listed in table 1. Now 13 modes are found for $c_r < 1$ lying along upper and lower lines, again only slightly displaced from their positions at $R = 1000$. These lines, although fictitious, are of great assistance in extrapolating the eigenvalues to

† These eigenvalues have now been calculated with high accuracy by Dr A. Davey (see Davey 1973 for the method used); by Dr D. J. R. Houston in association with Dr Jordinson using a modification of Jordinson's original finite-difference method; and by Dr H. Kümmerer, also using a finite-difference method.

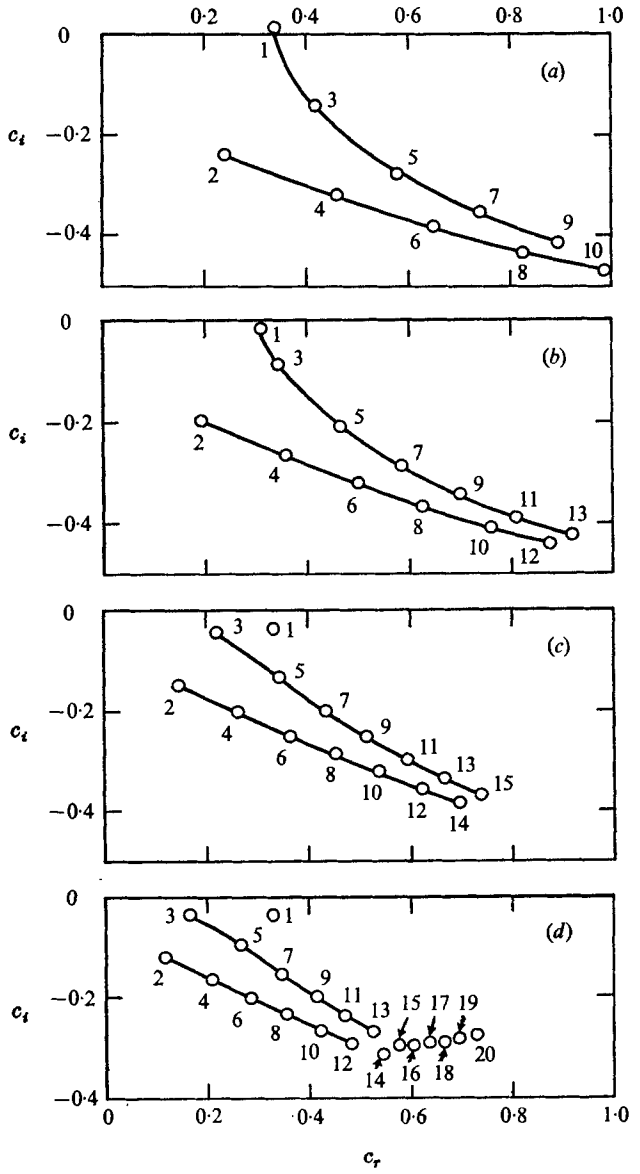

FIGURE 2. Distribution of eigenvalues of Blasius flow in c plane at $\alpha = 0{\cdot}179$ and four Reynolds numbers R: (*a*) 1000; (*b*) 2000; (*c*) 5000; (*d*) 10 000.

higher Reynolds numbers. Because their location in the c plane is only a slowly-varying function of R, they make it easy to follow the movement of the known modes as R increases. Even more important, the predictable spacing of the eigenvalues along each line makes it possible to find the new modes which move across $c_r = 1$ without recourse to the contour method. The first 11 modes were obtained with $y_1 = 8$, mode 12 with $y_1 = 10$ and mode 13 with $y_1 = 12$. Because of the round-off error problem mentioned in §2, convergence difficulties are present for

Mode	c_r	c_i	s	c_r	c_i	s	c_r	c_i	s
	$R = 580$			$R = 1000$			$R = 2000$		
1	0·3641	0·0080	0·100	0·3383	0·0048	0·050	0·3089	−0·0166	0·050
2	0·2897	−0·2769	0·050	0·2408	−0·2391	0·050	0·1918	−0·1961	0·050
3	0·4839	−0·1921	0·050	0·4155	−0·1425	0·050	0·3425	−0·0816	0·050
4	0·5572	−0·3653	0·050	0·4551	−0·3187	0·050	0·3553	−0·2648	0·050
5	0·6862	−0·3307	0·033	0·5773	−0·2730	0·050	0·4651	−0·2079	0·050
6	0·7936	−0·4341	0·033	0·6443	−0·3843	0·050	0·4986	−0·3214	0·050
7	0·8874	−0·4147	0·033	0·7341	−0·3569	0·050	0·5844	−0·2855	0·050
8	—	—	—	0·8193	−0·4348	0·050	0·6297	−0·3710	0·033
9	—	—	—	0·8890	−0·4154	0·025	0·6982	−0·3447	0·025
10	—	—	—	0·9889	−0·4686	0·033	0·7538	−0·4120	0·025
11	—	—	—	——	—	—	0·8092	−0·3905	0·025
12	—	—	—	—	—	—	0·8741	−0·4439	0·025
13	—	—	—	—	—	—	0·920	−0·426	0·033
	$R = 5000$			$R = 10\,000$					
1	0·3283	−0·0294	0·0500	0·3250	−0·0325	0·0250			
2	0·1429	−0·1484	0·0250	0·1144	−0·1190	0·0250			
3	0·2172	−0·0456	0·0500	0·1684	−0·0387	0·0250			
4	0·2603	−0·2037	0·0500	0·2070	−0·1653	0·0333			
5	0·3471	−0·1367	0·0500	0·2686	−0·0974	0·0250			
6	0·3604	−0·2491	0·0333	0·2847	−0·2013	0·0250			
7	0·4352	−0·2042	0·0250	0·3466	−0·1540	0·0250			
8	0·4519	−0·2893	0·0250	0·3552	−0·2363	0·0250			
9	0·5158	−0·2559	0·0250	0·4111	−0·1989	0·0250			
10	0·5375	−0·3256	0·0250	0·4209	−0·2667	0·0250			
11	0·5921	−0·2989	0·0250	0·4709	−0·2366	0·0250			
12	0·6188	−0·3580	0·0250	0·4828	−0·2952	0·0125			
13	0·6657	−0·3356	0·0250	0·5278	−0·2699	0·0125			
14	0·6971	−0·3872	0·0125	0·5469	−0·3129	0·0125			
15	0·7377	−0·3673	0·0125	0·5790	−0·2942	0·0125			
16	—	—	—	0·6058	−0·2948	0·0125			

TABLE 1. Eigenvalues of Blasius flow at $\alpha = 0{\cdot}179$

mode 13. The c listed in table 1 has only three significant digits, and $\phi(0)$ could not be reduced much below 0·001. Mode 14, which can be estimated by extrapolation to be at $c = (0{\cdot}990, -0{\cdot}475)$, could not be resolved at all.

With another increase of R to 5000, the 13 known modes were determined as at $R = 2000$ and two additional modes, 14 and 15, found by extrapolation along the upper and lower lines. The 15 modes are shown in figure 2(*c*) and listed in table 1. Attempts to locate additional modes by extrapolation failed. Because the oscillations of the viscous solution increase with Reynolds number and c_r, it was necessary to use a step size of 0·025 for the modes beyond six and of 0·0125 for modes 14 and 15 in order to have four-place accuracy. Convergence is again a problem for the last two modes. With $\Delta c = 0{\cdot}001$ the search procedure is consistent from iteration to iteration, but $\phi(0)$ could only be reduced to about 0·001.

However, there appear to be four significant figures in the eigenvalues rather than the three of mode 13 at $R = 2000$ for a similar value of $\phi(0)$.

At $R = 10\,000$ the 15 modes known at $R = 5000$ were readily determined and are shown in figure 2 (*d*) and listed in table 1. Modes 14 and 15 are slightly but definitely displaced upwards from the upper and lower lines and for this resaon the lines are terminated in figure 2 (*d*) at modes 12 and 13. Since modes 14 and 15 have at least one more significant figure than at $R = 5000$, and mode 16 could not be found by extrapolation, the contour method was used to find the next modes in the sequence. Five additional modes, 16–20, were found and are shown in figure 2 (*d*). In distinct contrast to the previous results, the new modes lie on a single straight line with a small positive slope. The change of pattern is so complete as to raise the possibility that modes 16–20 are spurious. In support of their reality, it can be pointed out that they are independent of y_1, and depend on the step size only to the extent of an improvement in the apparent accuracy as s becomes smaller. In addition, mode 16 was verified with the fixed step-size Adams–Moulton integrator with $s = 0{\cdot}01$. However, for larger s there is no indication at all of an eigenvalue. Since the Runge–Kutta integrator gives convergence for s as large as 0·025, it is perhaps not too surprising that modes 17–20 cannot be verified at all, even with s as small as 0·005. The verification of mode 16 does establish the change of pattern, but the failure to verify modes 17–20 makes it prudent to accept these modes only provisionally. Eigenvalue searches with different values of Δc give some idea of which digits are significant; and, according to this criterion, the eigenvalues of modes 16–20 all have 3–4 significant digits, apart from whatever influence the step size has.

All of the calculations that have been carried out for $\alpha = 0{\cdot}179$ are summarized in figures 3 (*a*) and (*b*) where c_r and c_i, respectively, are given as functions of R for $R > 10$. It can be noted from the figures that, except for behaviour connected with the fundamental mode, the mode order originally given in figure 1 by numbering with respect to c_r is preserved at all Reynolds numbers, while the odd-numbered c_i curves repeatedly cross the even-numbered. Below $R = 25$ only the fundamental mode exists, and below $R = 3{\cdot}9$ there are no modes at all.

As the Reynolds number increases all modes move towards $c = 0$ with the exception of mode 3. The c_r and c_i marked inv. in figure 3 were obtained from the author's inviscid stability program ISTAB for $\alpha = 0{\cdot}179$. An indented contour of integration was used, which passes under the singular point at $U = c$. Here U is the continuation by a truncated power series of the mean velocity U onto the complex y plane. This procedure follows from the demonstration by Lin (1955) that eigenvalues of the inviscid equation obtained in this manner are the $R \to \infty$ limit of eigenvalues of the Orr–Sommerfeld equation. The present calculation offers an example of the correctness of this technique, and also of the power of Gram–Schmidt orthonormalization to preserve linear independence at high Reynolds numbers. The inviscid eigenvalue was used as the initial guess in the viscous program at $R = 10^5$. Convergence to a viscous eigenvalue only slightly different from the inviscid eigenvalue was obtained in two iterations. When this eigenvalue was traced back to lower Reynolds numbers it was found to connect not with mode 1, the fundamental, but with mode 3. Thus, as figure 3 indicates,

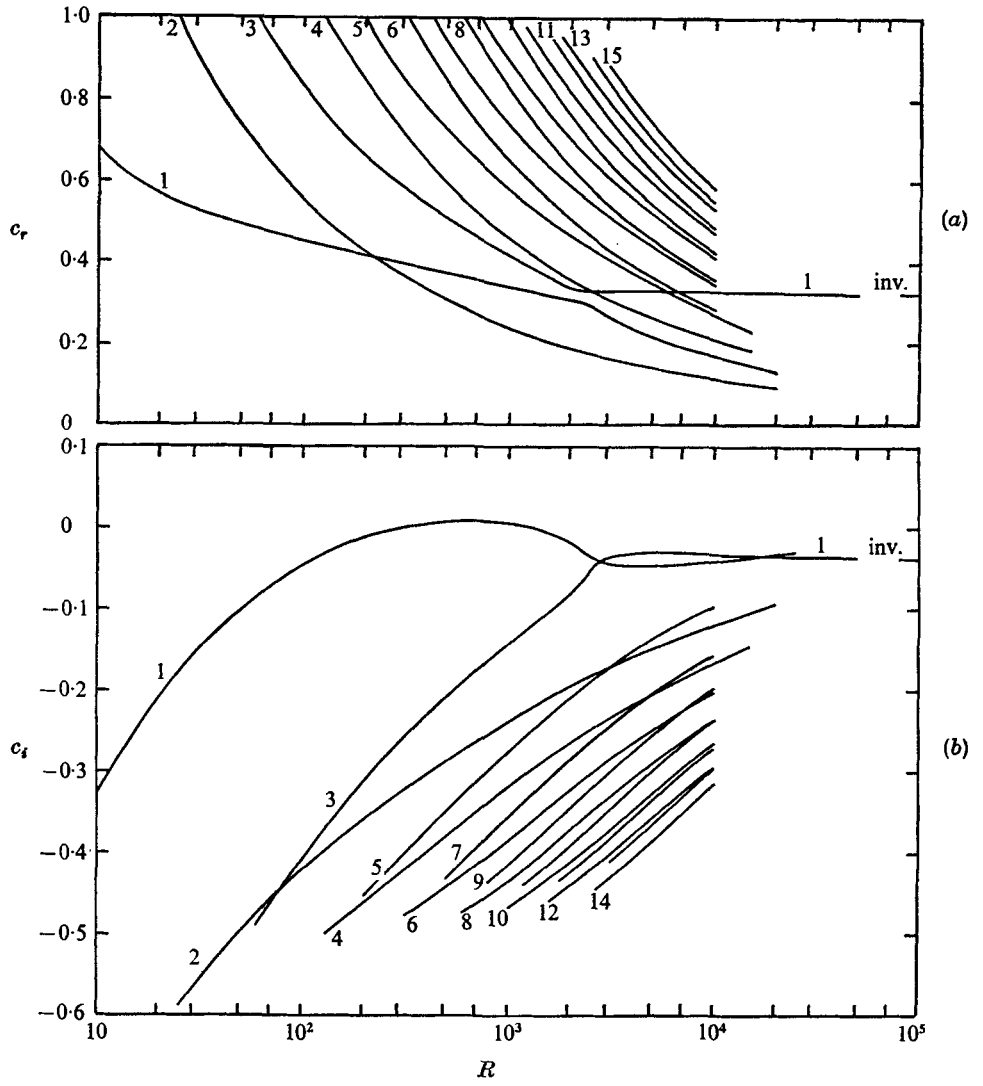

FIGURE 3. Effect of Reynolds number on c_r and c_i of the first 15 modes of Blasius flow at $\alpha = 0{\cdot}179$.

modes 1 and 3 switch identities between $R = 2000$ and 3000. That is, for R greater than about 2500, the point of closest approach of the two modes in figure 3, the curve that starts out as mode 3 at low R is actually mode 1 and vice versa. This change of identity has already been taken into account in labelling the modes in figures 2 (*c*) and (*d*). The appearance of figure 3 suggests that there is probably an α, R combination at which modes 1 and 3 actually intersect.

One mode, therefore, has an inviscid limit; but what of the others? The impression gathered from figure 3, of movement towards $c = 0$, is reinforced if c_r and c_i are plotted against R^{-1}. Furthermore, if the trajectories of the modes are plotted in the c plane, the first few modes seem clearly headed for the origin. It is useful

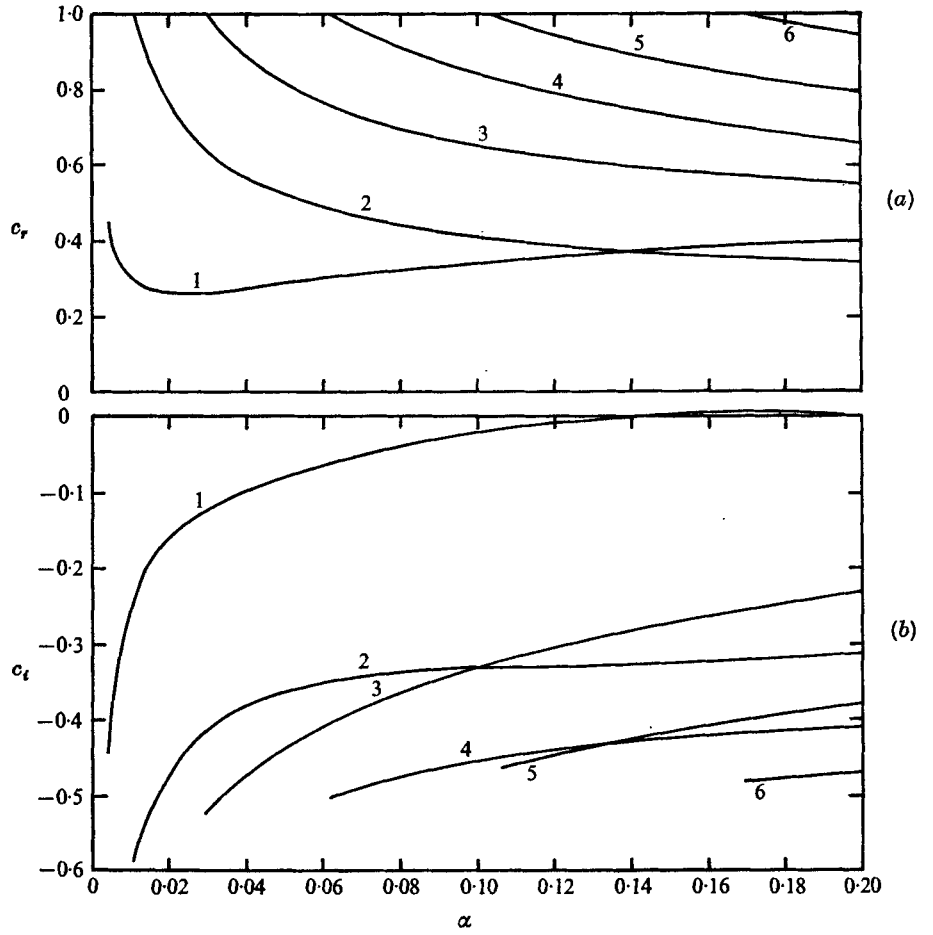

FIGURE 4. Effect of wavenumber on c_r and c_i of the first 6 modes of Blasius flow at $R = 337$.

to recall that Lin (1961) has shown that all viscous modes need not have an inviscid limit. Thus, no matter how closely a given mode may approach $c = 0$, or some other point, as R increases indefinitely, there is no requirement for this point to be an eigenvalue of the inviscid equation, or for the mode to take on an inviscid character as does mode 1. Even with Lin's technique, the only inviscid damped solution known to exist is the $R \to \infty$ limit of mode 1.

Finally, it remains to say something about the dependence of the eigenvalues on α. In figures 4 (a) and (b), the variation of c_r and c_i, respectively, with α is shown for $R = 337$ and $\alpha < 0{\cdot}2$. As α decreases, all modes, except possibly the fundamental, move out of the $c_r < 1$ region of the c plane, just as they do for decreasing R at fixed α. As also happens with changes in R, the order of the modes other than the fundamental is preserved in the numbering system with respect to c_r. In figure 4 (b), by contrast, the curves of even- and odd-numbered modes have different slopes and cross one another. Only for $\alpha < 0{\cdot}1$ does the order of the modes in terms of c_i correspond to the numbering system.

	$R = 580$		$R = 2000$		$R = 10\,000$	
Mode	$(\Delta E/E)_\delta$	$E(T)/E(0)$	$(\Delta E/E)_\delta$	$E(T)/E(0)$	$(\Delta E/E)_\delta$	$E(T)/E(0)$
1	0·0462	1·32	0·109	0·509	−0·194	0·285
2	−0·872	$6{\cdot}11\times10^{-6}$	−0·889	$2{\cdot}63\times10^{-6}$	−0·893	$2{\cdot}10\times10^{-6}$
3	−0·574	$6{\cdot}74\times10^{-3}$	−0·401	0·0501	−0·390	0·0557
4	−0·756	$2{\cdot}58\times10^{-4}$	−0·799	$8{\cdot}56\times10^{-5}$	−0·821	$4{\cdot}38\times10^{-5}$
5	−0·646	$2{\cdot}33\times10^{-3}$	−0·618	$3{\cdot}63\times10^{-3}$	−0·542	0·0105
6	−0·692	$1{\cdot}01\times10^{-3}$	−0·750	$3{\cdot}03\times10^{-4}$	−0·782	$1{\cdot}38\times10^{-4}$
7	−0·634	$2{\cdot}79\times10^{-3}$	−0·651	$2{\cdot}16\times10^{-3}$	−0·616	$3{\cdot}76\times10^{-3}$
8	—	—	—	$6{\cdot}09\times10^{-4}$	−0·761	$2{\cdot}34\times10^{-4}$
9	—	—	—	$2{\cdot}02\times10^{-3}$	−0·647	$2{\cdot}29\times10^{-3}$
10	—	—	—	$1{\cdot}04\times10^{-3}$	−0·744	$3{\cdot}48\times10^{-4}$

TABLE 2. Kinetic-energy change in distance δ and period T for 10 modes at $R = 580$, 2000, 10 000 and $\alpha = 0{\cdot}179$

As α increases above 0·2, modes 1 and 3 continue to approach each other until about $\alpha = 0{\cdot}30$ for c_r and $\alpha = 0{\cdot}45$ for c_i, after which they slowly diverge. Since the c_r of mode 3 is close to the inviscid eigenvalue computed by Lin's technique for $\alpha > 0{\cdot}45$ in spite of the low Reynolds number, it can be concluded that modes 1 and 3 again change identity, as they do with increasing R at constant α. The behaviour is clearer at $R = 5000$, which for $\alpha = 0{\cdot}179$ is above the Reynolds number where the identity change takes place ($R \approx 2500$). For $\alpha > 0{\cdot}179$ both c_r and c_i of mode 1 (mode 3 below $R = 2500$) follow almost exactly the inviscid eigenvalues. Mode 3 (mode 1 below $R = 2500$) has a constant c_i for $\alpha > 0{\cdot}15$ up to the limit of the calculations at $\alpha = 0{\cdot}26$. Both the c_r and c_i curves of modes 1 and 3 cross one another at $\alpha = 0{\cdot}14$ and 0·21, respectively, but there is no change of identity, and neither of these points is a point of degeneracy.

3.3. *Physical properties of the modes*

As is evident from table 1, all of the modes except mode 1 are highly damped. For example, the least-damped additional mode, mode 3, has a damping rate at $R = 580$ which is 24 times greater than the amplification rate of mode 1. In order to bring out the consequences of such high damping rates, it is helpful to introduce the dimensionless mean kinetic energy of a disturbance

$$E = \tfrac{1}{2}(\langle u'^2\rangle + \langle v'^2\rangle). \tag{21}$$

A prime now refers to a fluctuation, and $\langle\ \rangle$ to an average over a wavelength. The reference energy is $\rho^* U_1^{*2}$; ρ^* is the density. The fractional energy change in $t^* = \delta/c_r^*$, the time required for a disturbance of phase velocity c_r^* to advance one boundary-layer thickness δ, is

$$(\Delta E/E)_\delta = \exp(2\alpha y_\delta c_i/c_r) - 1. \tag{22}$$

$y_\delta = \delta R/x^*$ is the Blasius variable evaluated at δ. The value of y_δ is 6·011 when δ is defined as the y^* where $U = 0{\cdot}999$. Another measure of energy change is the

	1	2	3	4	5	6	7
$P/\lvert\dot{E}\rvert$	2·92	−0·395	−0·651	−0·151	−0·148	−0·068	−0·046
$V/\lvert\dot{E}\rvert$	1·90	0·606	0·357	0·849	0·852	0·932	0·954
$\Delta/\lvert\dot{E}\rvert$	−0·02	0·002	0·008	—	—	—	—

TABLE 3. Contribution to integrated energy loss (or gain) of production and viscous dissipation terms, $R = 580$, $\alpha = 0{\cdot}179$

ratio of the energy after one period T^*, $E(T^*)$, to the initial energy $E(0)$. This is

$$E(T^*)/E(0) = \exp(4\pi c_i/c_r). \tag{23}$$

The above two energy ratios are listed in table 2 for the first 10 modes at $R = 580$, 2000, 10000 and $\alpha = 0{\cdot}179$. While the Tollmien–Schlichting wave increases its energy at $R = 580$ by 4·6 % every boundary-layer thickness, and by 32 % every cycle, all of the damped disturbances except mode 3 lose over 99 % of their energy in a single cycle, and from 54 % to 89 % in one boundary-layer thickness. Even the least-damped additional mode, mode 3, retains only about 5 % of its initial energy at $R \geqslant 2000$ after one cycle. As an indication of how rapidly even a low damping rate depletes energy, mode 1, which has a damping rate at $R = 2000$ about double the amplification rate at $R = 580$, loses 49 % of its energy in a single cycle.

The sources of the energy change can be identified by integrating the local kinetic-energy equation from $y = 0$ to y_1 to yield

$$P - V + \Delta = \dot{E}. \tag{24}$$

In (24), $\dot{E}$ is the change of the integrated kinetic energy per unit time, P is the energy produced by the Reynolds stress, V is the disturbance viscous dissipation, and Δ consists of pressure–velocity and shear stress–velocity correlations. If $c_r \neq 1$, $\Delta \to 0$ as $y_1 \to \infty$. The three ratios $P/\lvert\dot{E}\rvert$, $V/\lvert\dot{E}\rvert$ and $\Delta/\lvert\dot{E}\rvert$ are listed in table 3 for the seven modes of figure 1, and were obtained by numerical integration from $y = 0$ to $y_1 \doteq 12$ of the terms of the local energy-balance equation.

Table 3 serves to emphasize the disparity between mode 1 and the damped modes. For mode 1, three times as much energy as is gained by the disturbance is produced by the Reynolds stress, and two-thirds of this energy is lost to viscous dissipation. In contrast, for the other modes energy is lost both by the action of the Reynolds stress and by dissipation. For mode 3, 65 % of the energy loss is from the Reynolds stress, an amount that decreases to 5 % for mode 7. An interesting feature concerning the viscous dissipation is that as the mode number increases the ratio of the local viscous dissipation V_y to the local kinetic energy E_y becomes important over more and more of the boundary layer and also tends to be distributed more uniformly. The y^*/δ within which $V_y/E_y > 0{\cdot}1$ increases from 0·6 for mode 4 to greater than 2·0 for mode 7.

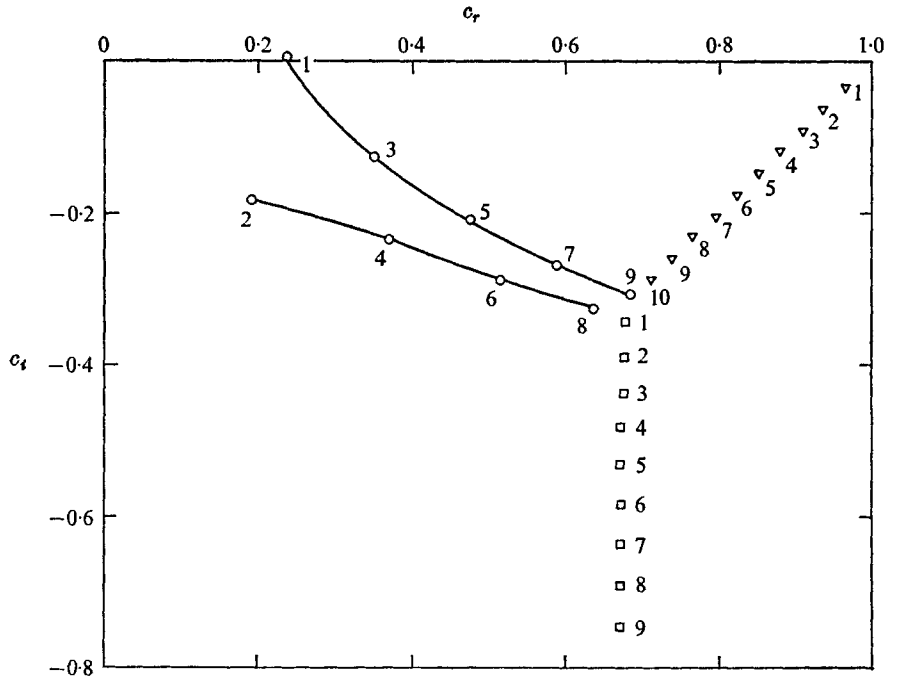

FIGURE 5. Distribution of eigenvalues of antisymmetric disturbances for plane Poiseuille flow at $\alpha = 1{\cdot}0$, $R = 10\,000$. ⊙, A family; ▽, P family; ⊡, S family.

4. Eigenvalues of flows with two boundaries

4.1. *Plane Poiseuille flow*

In an effort to understand why so few eigenvalues were found in the calculations of §3, it will be instructive to examine the eigenvalue spectrum of plane Poiseuille flow, which is known to be infinite. Orszag (1971) has accurately computed the first 17 temporal modes of antisymmetric disturbances (even stream function) at $\alpha = 1{\cdot}0$, $R = 10\,000$ (here $L^* = H^*$, the half-width of the channel), and the first 15 modes of symmetric disturbances (odd stream function). His calculations of antisymmetric disturbances have been extended by the contour method together with the linear search procedure to larger values of $-c_i$, and these results are shown together with Orszag's in figure 5 and listed in table 4. The eigenvalues have been classed by the present author into three families, A, P and S. The more usual mode number n, based on arranging the eigenvalues in order of decreasing c_i, is also listed in column 2 of this table.

The nine members of the A family are distributed along upper and lower lines which are not far removed from the similar lines of figure 2. As indicated by figure 6, where portions of the $D_r = 0$, $D_i = 0$ contours are sketched in the region $0{\cdot}5 < c_r < 1$, $-0{\cdot}4 < c_i < -0{\cdot}1$, the contour patterns for modes A 1–A 8 are close to the patterns in figure 1. (Compare modes 4–6 of figure 1 with modes A 6–A 8 in figure 6.) A 9 is a transitional mode that could perhaps have been assigned to either the P or S families; but, since it fits the spacing of the A family rather than either of the other families, it has been classified with the A family. The contours

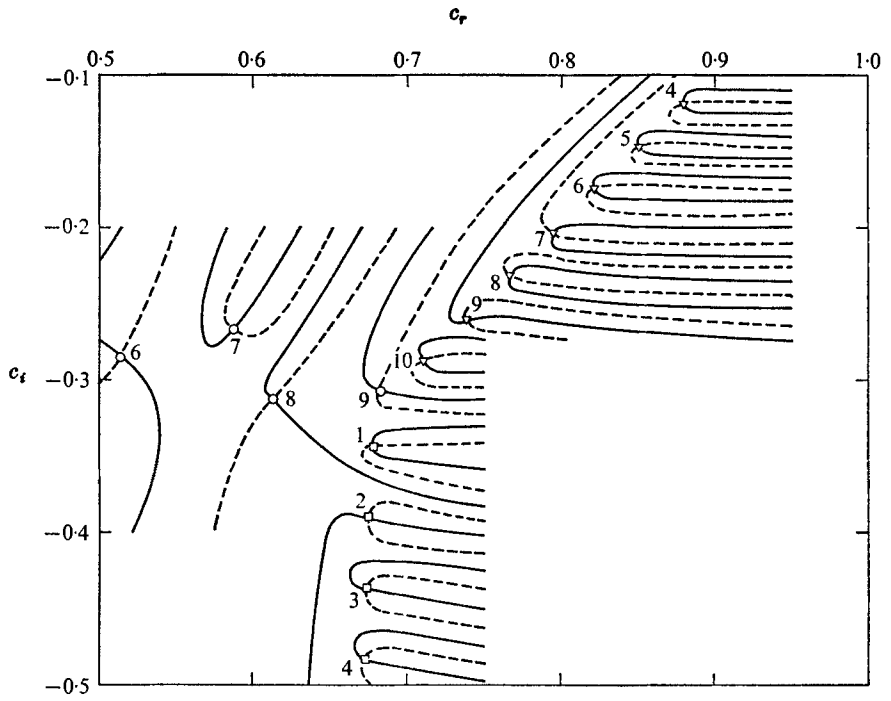

FIGURE 6. Zero contour lines of secular determinant for plane Poiseuille flow at $\alpha = 1{\cdot}0$, $R = 10\,000$: ——, $D_r = 0$; – – –, $D_i = 0$. ⊙, A family; ▽, P family; ⊡, S family.

for the P and S modes are an entirely new feature, and bear no relation to anything in figure 1. They either originate or end at $c_r = 1$, and for the most part do both. Except near the intersection points they form a periodic sequence of lines roughly parallel to the c_r axis.

The appearance of figure 5 would by itself suggest classifying the eigenvalues into different groups, but theoretical support is also available. Schensted (1960) not only demonstrated that the spectrum is infinite, but also succeeded in deriving approximate formulae for three distinct families of eigenvalues. One family, which had originally been obtained by Pekeris (1948), is almost exactly the family denoted here by the letter P and calculated by Orszag (1971). A second family is perhaps related to the A family, although it lies on only a single line, and the third family, which unlike the first two is infinite in extent, is the asymptotic representation of what is labelled here as the S family. According to Schensted, $c_i = -n^2\pi^2/\alpha R$ for this family, and c_r is unspecified. The last mode calculated, S 14 ($n = 33$), is within 2 % of this value, but even closer agreement is given by the formula $-(4n-1)^2/16\alpha R$, which was derived by Grosch & Salwen (1968) in their extensive study of the spectrum of plane Poiseuille flow. The c_i given by this latter formula is listed in column 5 of table 4. The asymptotic value of c_r according to Grosch & Salwen is $\frac{2}{3}$, the average velocity of the mean flow in the channel.

Mode	n	c_r	c_i	$\frac{-(4n-1)^2\pi^2}{16\alpha R}$
P 1	2	0·96464	−0·03519	—
P 2	3	0·93635	−0·06325	—
P 3	4	0·90806	−0·09131	—
P 4	5	0·87976	−0·11937	—
P 5	7	0·85145	−0·14743	—
P 6	8	0·82314	−0·17548	—
P 7	10	0·79482	−0·20353	—
P 8	12	0·76649	−0·23159	—
P 9	14	0·73812	−0·25965	—
P 10	17	0·70887	−0·28769	—
A 1	1	0·23753	+0·00374	—
A 2	9	0·19006	−0·18282	—
A 3	6	0·34911	−0·12450	—
A 4	13	0·36850	−0·23382	—
A 5	11	0·47490	−0·20873	—
A 6	15	0·51292	−0·28663	—
A 7	16	0·58721	−0·26716	—
A 8	19	0·63610	−0·32519	—
A 9	18	0·68286	−0·30761	—
S 1	20	0·67759	−0·34373	−0·3850
S 2	21	0·67451	−0·38983	−0·4249
S 3	22	0·67321	−0·43580	−0·4669
S 4	23	0·67232	−0·48326	−0·5108
S 5	24	0·67159	−0·53241	−0·5567
S 6	25	0·67097	−0·58327	−0·6046
S 7	26	0·67043	−0·63588	−0·6549
S 8	27	0·66997	−0·69025	−0·7062
S 9	28	0·66957	−0·74642	−0·7600
S 10	29	0·66923	−0·80439	−0·8158
S 11	30	0·66894	−0·86418	−0·8735
S 12	31	0·66868	−0·92582	−0·9332
S 13	32	0·66846	−0·98932	−0·9949
S 14	33	0·66826	−1·05468	−1·0586

TABLE 4. Eigenvalues of antisymmetric disturbances of plane Poiseuille flow at $\alpha = 1{\cdot}0$, $R = 10\,000$ (n = 1–17 from Orszag 1971)

4.2. *Artificial flows with* $H \to \infty$

Schensted (1960) proved that any channel flow has an infinite discrete spectrum but there is no such general result for a flow with a single boundary. In order to gain deeper understanding of the difference between the spectra for finite and infinite intervals, two artificial flows will be considered, in which the upper boundary moves to $y \to \infty$. The emphasis will be on how the S family changes with H, the channel width. It is the absence of the S family and the related P family that distinguishes the Blasius spectrum from that for Poiseuille flow. The A modes are present in both flows. Figure 6 provides the essential information needed to carry out the investigation in a straightforward manner. Since the S modes are associated with the periodic sequence of nearly parallel contours, all that is necessary is to look for periodicity in D_r and D_i as c_i varies for some fixed c_r

over a range of c_i less than, say, $-0{\cdot}4$. If periodicity is found, then S modes must exist somewhere to the left of the chosen c_r.

The first artificial flow consists of a parabolic velocity profile $1-(1-y)^2$ for $0 < y < 1$ and $2H-1 < y < 2H$, and a uniform flow between $y = 1$ and $y = 2H-1$. H will be varied from 2 to 8 with α and R based on L^*, the height of the shear flow, remaining constant. A fairly complete contour pattern has been worked out for $H = 2$ in order to get oriented and it is somewhat more complicated than figure 6. The A family, except for A 9, is only slightly displaced from its location at $H = 1$, but the P family lies along two lines rather than one. The all-important S family is shifted right to about $c_r = 0{\cdot}75$, with an initial spacing not much different from that with $H = 1$. No actual eigenvalues were computed with the linear search procedure in the calculations to be discussed in the remainder of this section, so the locations referred to are only approximately determined intersection points. The main new feature present with $H = 2$ is another family of eigenvalues with a c_r which decreases from 0·98 near $c_i = -0{\cdot}1$ to 0·95 for $c_i < -0{\cdot}3$. The calculations did not extend below $c_i = -0{\cdot}5$. For $c_i < -0{\cdot}3$ the contour spacing at $c_r = 1$ is only one-half what it is to the left of the new family, and the extra contours turn back to $c_r = 1$ at the intersection points which form these eigenvalues.

With an increase of H to 4, the main part of the contour pattern remained virtually unchanged. Consequently, $H = 2$ is already close to the asymptotic state, as was verified by calculations with $H = 8$. However, there is an important change in the eigenvalue family near $c_r = 1$ as H increases. The spacing of the contours at $c_r = 1$ is inversely proportional to H, thus the number of eigenvalues increases with H. At the same time, the eigenvalues move closer to $c_r = 1$. This behaviour is discussed more fully below, where it reappears in a somewhat different guise.

The second artificial flow consists of a Blasius velocity profile arranged symmetrically about the channel centre-line at $y = H$, where L^* is now the Blasius length scale. With H large and y_1 also large to check whether the results are independent of y_1, the asymptotic form of $U(y)$ given by (19) can be used for the outer part of the profile, or the profile can be truncated at some arbitrary large y and $U = 1$, $U' = 0$ used from that point to the symmetry axis. Equivalent results were found from either method for a truncation y greater than 8. H was varied from 8 to 60, and the calculations were restricted for the most part to finding periodicity in D_r and D_i for $c_i < -0{\cdot}4$, thereby locating the start of the S family of eigenvalues.

In the first calculation, with $H = 8$, the sought-for periodic sequence of zeros of D_r and D_i was found at $c_r = 0{\cdot}82$ for c_i between $-0{\cdot}4$ and $-0{\cdot}6$ where the calculations ceased. The contours are indeed nearly parallel lines for $c_r \geqslant 0{\cdot}82$, and the curves come together to form four intersections at about $c_r = 0{\cdot}79$. These intersection points are interpreted to be S-family eigenvalues. With H increased to 10, there is no longer periodicity at $c_r = 0{\cdot}82$. An isolated intersection was found near $c = (0{\cdot}79, -0{\cdot}43)$, which is of the same type and at almost exactly the location of mode 6 in figure 1. For $c_r > 0{\cdot}86$ there is again a periodic sequence of parallel lines, from $c_i = -0{\cdot}4$ to at least $-0{\cdot}7$, which form an S family

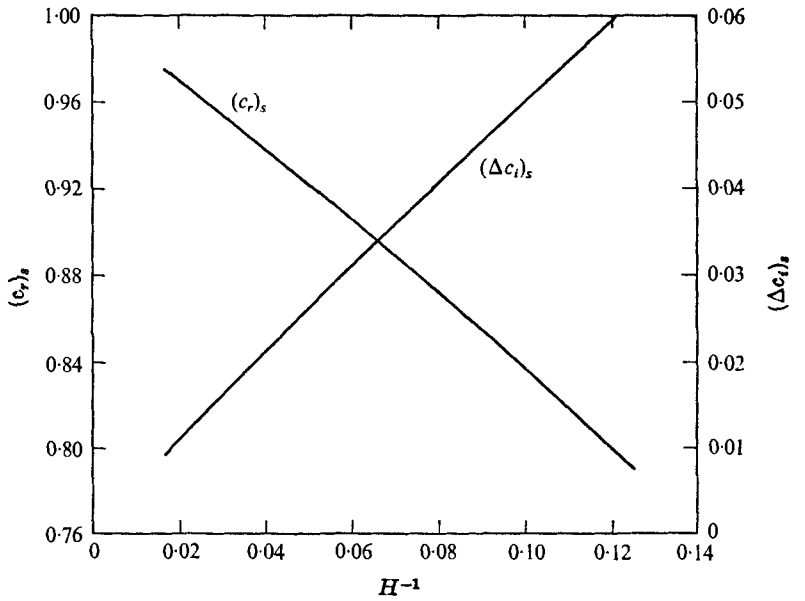

FIGURE 7. Effect of channel width on S-family eigenvalues of flow made up of two Blasius boundary layers: $\alpha = 0{\cdot}179$, $R = 580$.

intersection at a c_r of about 0·83. Unlike the first artificial flow, the spacing of the contours remains unchanged all the way to $c_r = 1$, so there is no second family of eigenvalues near $c_r = 1$.

As H is increased further, the S family does not reach an asymptotic state at some $c_r < 1$, but continues to move towards $c_r = 1$, while at the same time the spacing between the eigenvalues decreases. The c_r of the intersections, denoted by $(c_r)_s$, and the spacing, denoted by $(\Delta c_i)_s$, have been plotted in figure 7 against H^{-1} from $H = 8$ to 60. It is fairly easy to obtain $(c_r)_s$, because it is almost independent of c_i, at least up to the limit of the calculations at $c_i = -1$, but $(\Delta c_i)_s$ is more problematical because of its unknown dependence on c_i. The $(\Delta c_i)_s$ of the figure is intended to represent an average spacing in the region $-0{\cdot}8 < c_i < -0{\cdot}6$. In any case the tendency is clear: $(c_r)_s \to 1$ and $(\Delta c_i)_s \to 0$ as $H \to \infty$. Thus, the S family acts not as it did for the first artificial flow with a parabolic velocity profile, but like the additional family of eigenvalues that appeared near $c_r = 1$ with $H > 1$. It should be pointed out that a non-uniform limit is involved here. For any $c_r < 1$, an asymptotic state with no periodicity can be achieved by making H sufficiently large, but the required H increases indefinitely as $c_r \to 1$. At $c_r = 1$ there is no limit. The two viscous solutions do not diminish in amplitude as y (or $2H - y$) increases, and the two-wall problem does not reduce to the one-wall problem as $H \to \infty$. Consequently, whatever takes place at $c_r = 1$ as $H \to \infty$ has no application to the boundary-layer problem. What can be said is that, in complete agreement with figure 1, no part of the infinite discrete spectrum of the finite interval exists in the region $c_r < 1$, $c_i > -1$ as $H \to \infty$, nor does it approach a continuous spectrum anywhere in this region.

5. Other flows with a single boundary

The existence of the S family for a parabolic velocity profile, and its absence in the same limit for the Blasius profile, suggest an investigation into the influence of the profile on the spectrum for flows with a single boundary. This is limited here to profiles that can be described analytically, and to the initial part of the S family of eigenvalues. The most obvious difference between a parabolic and a Blasius profile is that in the latter all derivatives of U go to zero as $y \to \infty$, while in the former U'' is discontinuous at $y = 1$. This feature will provide the focal point of the following investigation.

According to (19), $U' \sim \exp(-y^2)$ in the outer part of the Blasius boundary layer. If the profile is simply truncated at $y = 8$, no effect at all on the results could be found. The asymptotic suction profile $U = 1 - \exp(-y)$ also has all derivatives approaching zero as $y \to \infty$, but at a slower rate. However, the result is the same: for sufficiently large H, there is no periodicity in D_r and D_i in the region where the S modes might be present.

The other profiles studied all belong to two families of polynomials. The first family is $U = 1-(1-y)^m$, which for $m = 2$ is the parabolic profile of §4. With this profile and no upper boundary, the S modes for $\alpha = 1{\cdot}0$, $R = 10\,000$ are the same as in the two-wall problem for $H \geqslant 2$ in the region covered by the calculations between $c_i = -0{\cdot}4$ and $-0{\cdot}8$. The spacing is about the same as for Poiseuille flow, but one difference is that c_r increases with increasing mode number instead of decreasing. Thus, c_r goes from 0·74 near $c_i = -0{\cdot}4$ to 0·77 near $c_i = -0{\cdot}8$. As the polynomial degree m increases above two, the mode closest to $c_i = -0{\cdot}4$ shifts to the right: $c_r = 0{\cdot}81$ for $m = 3$, and $c_r = 0{\cdot}87$ for $m = 4$. This shift is in accord with the expectation that a smoother profile at $y = 1$ might give results closer to true boundary-layer profiles.

A better approximation to a boundary layer is provided by the Pohlhausen method polynomials. For flat-plate flow the cubic, quartic and quintic profiles are

$$U = \begin{cases} 1{\cdot}5\bar{y} - 0{\cdot}5\bar{y}^3, \\ 2\bar{y} - 2\bar{y}^3 + \bar{y}^4, \\ 2{\cdot}5\bar{y} - 5\bar{y}^3 + 5\bar{y}^4 - 1{\cdot}5\bar{y}^5, \end{cases} \qquad \delta = \begin{cases} 4{\cdot}6410, \\ 5.8356, \\ 7{\cdot}0356, \end{cases} \qquad \delta^* = \begin{cases} 1{\cdot}7404, & (25) \\ 1{\cdot}7507, & (26) \\ 1{\cdot}7589, & (27) \end{cases}$$

$\bar{y} = y/\delta$, and δ and δ^* are the boundary-layer thickness and displacement thickness, respectively, in Blasius units. The calculations were performed at $\alpha = 0{\cdot}179$, $R = 580$ as for the Blasius profile.

With the cubic, two eigenvalues were found in the interval $-0{\cdot}6 < c_i < -0{\cdot}4$ at about $c = (0{\cdot}73, -0{\cdot}45)$ and $(0{\cdot}75, -0{\cdot}53)$. These eigenvalues are accepted as S modes because their contour pattern is the same as for the S family in figure 6. With the quartic, the eigenvalues move to about $c = (0{\cdot}84, -0{\cdot}48)$ and $(0{\cdot}85, -0{\cdot}56)$. Finally, with the quintic five eigenvalues were found between $c_i = -0{\cdot}4$ and $-0{\cdot}8$ at $c_r = 0{\cdot}90$, 0·91, 0·92, 0·93 and 0·94. The rapid progression of these modes towards $c_r = 1$ suggests that their number may not be infinite, although a similar movement occurs for the parabolic profile with $H \geqslant 2$ in the two-wall

problem where the spectrum is known to be infinite. Unfortunately, the inability to integrate near $c_r = 1$ for $c_i < -0{\cdot}8$ precluded any further investigation.

What this limited study shows is that there are approximate boundary-layer profiles that have at least a remnant of the S family of eigenvalues. As the profile becomes more realistic in the sense of having more zero derivatives at the outer edge of the boundary layer, these eigenvalues move towards $c_r = 1$. A reasonable inference is that any real boundary-layer profile, in which all derivatives go to zero as $y \to \infty$, will give a result similar to that for the Blasius and asymptotic suction profiles (i.e. no infinite discrete spectrum for $c_r < 1$ of the type that exists for channel flows).

6. Concluding remarks

The mathematical questions of whether the eigenvalue spectrum of the Blasius boundary layer is infinite and the eigenfunctions complete cannot be answered definitively by a numerical investigation. What the latter can do, besides the actual calculation of certain eigenvalues, is to narrow the range of possibilities. If it is accepted that all discrete eigenvalues will be given by the intersections of the zero contour lines as in figures 1 and 6, then it has been shown that, for the conditions of figure 1, the only such eigenvalues in the region $0 < c_r < 2, c_i > -3$ are the seven modes listed in table 1 and shown in figure 1. The calculations of § 4 for the two-wall flow with Blasius boundary layers support this conclusion, by showing that (at least for $c_i > -1$) the finite-interval eigenvalues of the S family can be moved to $c_r > k$, where k is any $c_r < 1$, by making the channel width $2H$ sufficiently large.

This suggests a close look at $c_r = 1$ as a possible locus of additional eigenvalues. Since λ_3 and λ_4 are pure imaginary for $c_r = 1$, $c_i < -\alpha/R$ according to (9), the viscous solutions are periodic in y and extend to infinity with constant amplitude. With two walls, there is a discontinuous limit involved, so that $H \to \infty$ with $c_r < 1$ and $H \to \infty$ with $c_r = 1$ are fundamentally different. Therefore, figure 7 cannot be interpreted as showing a continuous spectrum for the two-wall problem at $c_r = 1$ in this limit. Indeed, the symmetry condition imposed severely restricts the possibilities, and there is no reason to expect a continuous spectrum when the viscous solutions differ only in phase. For any value of H, no matter how large, there will always be an infinite discrete spectrum in the $c_r < 1$ part of the complex plane, with the location and spacing of the eigenvalues given by figure 7. For arbitrarily large H, the modes are arbitrarily close to one another, but they are still discrete and do not form a continuum. When $H \to \infty$ with $c_r = 1$, a limiting state is quickly reached as soon as the influence of the second *inviscid* solution is negligible. There are only phase changes as the upper wall moves further away, and the numerical calculations show no evidence of eigenvalues along $c_r = 1$ under these conditions.

Once the discrete spectrum of Blasius flow is accepted as finite, the only possibility of representing an arbitrary disturbance by a superposition of eigenvalues is for there to be a continuous spectrum somewhere. The numerical results would seem to allow $c_r = 1, c_i < -\alpha/R$ as the only real possibility for the location of such

a spectrum. For these values of c_r and c_i, both viscous solutions satisfy the outer boundary condition of boundedness, and with an infinite interval there is no longer a symmetry condition to restrict the relative amplitudes of the two solutions. With three solutions available to satisfy two homogeneous boundary conditions at the wall, there cannot fail to be a continuous spectrum. Even with boundary-layer profiles which are discontinuous at $y = \delta$, so that there is an infinite discrete spectrum, there would still be a continuous spectrum at $c_r = 1$. Only an argument which rules out the use of the second viscous solution, or restricts its amplitude with respect to the first viscous solution, would also rule out the continuous spectrum.

The program VSTAB contains an option developed for sound interaction problems in supersonic flow that permits the magnitude of any solution, either viscous or inviscid, to be specified, then calculates the magnitudes of the solutions normally used to find discrete eigenvalues such that a linear combination of the three solutions satisfies the wall boundary conditions. Accordingly, with $c_r = 1$ the magnitude of the λ_3 solution was fixed and the magnitudes of the λ_1 and λ_4 solutions calculated for a range of $c_i < -\alpha/R$ with $\alpha = 0{\cdot}179$, $R = 580$. Incidentally, with both the λ_3 and λ_4 solutions present, the orthonormalization procedure removes the round-off error problem mentioned in §2 for large $-c_i$ with only the λ_3 solution. The results show that as $c_i \to -\alpha/R$ from below, the amplitude ratio of the two viscous solutions approaches unity, but for all other $c_i < -\alpha/R$, the amplitude of the λ_4 solution is smaller than that of the λ_3 solution. When $c_i = -2\alpha/R$, the ratio is $0{\cdot}7795$; at $-200\alpha/R$, it is $7{\cdot}650 \times 10^{-3}$; and at $-2000\alpha/R$, it is $1{\cdot}807 \times 10^{-9}$. These are free-stream ratios; at the wall, the two solutions are of comparable magnitude because of the behaviour mentioned in §2 after (18).

To summarize, the numerical results presented here support the following conclusions. For a finite interval, no matter how large, there is always an infinite discrete spectrum of eigenvalues whose spacing decreases indefinitely as the interval height increases. For an infinite interval, the discrete spectrum is finite, with the number of eigenvalues increasing as either the Reynolds number or wavenumber increases. In addition, there is a continuous spectrum located along the $c_r = 1$ axis for $c_i < -\alpha/R$. Mathematical proofs and a physical interpretation of the continuous spectrum remain to be given. In particular, the physical realization of the lightly-damped portion of the continuous spectrum could have important consequences for the behaviour of disturbances in a boundary layer.

I wish to thank Dr A. Davey for a most helpful and stimulating correspondence during the preparation of this paper, and also both him and Dr R. Jordinson as well as Dr H. Kümmerer for making unpublished computations available to me. Particular thanks are due to Dr H. Salwen and Dr C. E. Grosch for their insistence on the propriety of using both viscous solutions at $c_r = 1$ to form the continuous spectrum. This work represents the results of one phase of research carried out at the Jet Propulsion Laboratory, California Institute of Technology, under contract NAS7-100, sponsored by the National Aeronautics and Space Administration.

REFERENCES

BETCHOV, R. & CRIMINALE, W. O. 1967 *Stability of Parallel Flows*. Academic.

BLASIUS, H. 1908 Grenzschichten in Flüssigkeiten mit kleiner Reibung. *Z. Math. Phys.* 56.

DAVEY, A. 1973 A simple numerical method for solving Orr–Sommerfeld problems. *Quart. J. Mech. Appl. Math.* **26**, 401.

DAVEY, A. & DRAZIN, P. G. 1969 The stability of Poiseuille flow in a pipe. *J. Fluid Mech.* **36**, 209.

DIPRIMA, R. C. & HABETLER, G. J. 1969 A completeness theorem for non-selfadjoint eigenvalue problems in hydrodynamic stability. *Arch. Rat. Mech. Anal.* **34**, 218.

GALLAGHER, A. P. & MERCER, A. M. 1964 On the behaviour of small disturbances in plane Couette flow. *J. Fluid Mech.* **18**, 350.

GROSCH, C. E. & SALWEN, H. 1968 The stability of steady and time-dependent plane Poiseuille flow. *J. Fluid Mech.* **34**, 177.

JORDINSON, R. 1971 Spectrum of eigenvalues of the Orr–Sommerfeld equation for Blasius flow. *Phys. Fluids*, **14**, 2535.

KÜMMERER, H. 1973 Numerische Untersuchungen zur Stabilität ebener laminarer Grenzschichtströmungen. Dr. rer. nat. thesis, Universität Stuttgart.

LIN, C. C. 1955 *The Theory of Hydrodynamic Stability*, chap. 8. Cambridge University Press.

LIN, C. C. 1961 Some mathematical problems in the theory of the stability of parallel flows. *J. Fluid Mech.* **10**, 430.

MACK, L. M. 1965 Computation of the stability of the laminar compressible boundary layer. *Methods of Computational Physics*, vol. 4. Academic.

ORSZAG, S. A. 1971 Accurate solution of the Orr–Sommerfeld stability equation. *J. Fluid Mech.* **50**, 689.

PEKERIS, C. L. 1948 Stability of the laminar parabolic flow of a viscous fluid between parallel fixed walls. *Proc. Nat. Acad. Sci. Wash.* **34**, 285.

RAETZ, C. S. 1966 A further development of the resonance theory of transition including a correlation with an experiment. *Air Force Flight Dyn. Lab. Tech. Rep.* no. 66–192.

SALWEN, H. & GROSCH, C. E. 1972 The stability of Poiseuille flow in a pipe of circular cross-section. *J. Fluid Mech.* **54**, 93.

SCHENSTED, I. V. 1960 Contributions to the theory of hydrodynamic stability. Ph.D. thesis, University of Michigan.